INORGANIC CHEMISTRY
FRONTIERS

RESEARCH ARTICLE

View Article Online
View Journal | View Issue

Cite this: *Inorg. Chem. Front.*, 2022, **9**, 5064

Robust metal–organic framework with abundant large electronegative sites for removal of CO_2 from a ternary $C_2H_2/C_2H_4/CO_2$ mixture†

Cheng Xiong,‡[a] Yan-Hong Xiao,‡[a] Qingyou Liu,[b] Ling Chen,[a] Chun-Ting He,[a] Qing-Yan Liu *[a] and Yu-Ling Wang *[a]

Received 2nd June 2022,
Accepted 8th August 2022

DOI: 10.1039/d2qi01175a

rsc.li/frontiers-inorganic

Separation of ternary gas mixtures is challenging and has rarely been achieved with a single porous solid material. Herein a trinuclear iron(III) based metal–organic framework (MOF) with high water stability, $\{[Fe_3(\mu_3\text{-}O)(DFBDC)_3(TPT)](OH)\}_n$ (JXNU-14) ($DFBDC^{2-}$ = 2,5-difluoroterephthalate and TPT = 2,4,6-tri(4-pyridinyl)-1,3,5-triazine), is applied for the removal of CO_2 from a ternary $C_2H_2/C_2H_4/CO_2$ mixture. The trigonal bipyramidal cavities and cylindrical cavities decorated with highly electronegative fluorine and oxygen atoms and abundant π rings in JXNU-14 offer stronger affinity for C_2H_2 and C_2H_4 than for CO_2, resulting in the high-performance separation of a ternary equimolar mixture of C_2H_2, C_2H_4, and CO_2, which is demonstrated by pure-component gas adsorption isotherms and actual column breakthrough experiments. The much stronger binding of C_2H_2 and C_2H_4 as compared to CO_2 was further revealed by computational simulations. This work provides a useful strategy for the construction of MOFs possessing high-density electronegative sites for the efficient removal of CO_2 from a ternary $C_2H_2/C_2H_4/CO_2$ mixture.

Introduction

Metal–organic frameworks (MOFs), also termed porous coordination polymers (PCPs), built from organic ligands and metal ions through coordination bonds, are a kind of porous solid material.[1–3] Because of their highly fascinating structures and diverse functionalities, MOFs are used in a wide range of applications including sensing,[4] catalyses,[5,6] drug delivery,[7] proton conduction,[8–10] and gas storage and separation.[11–14] As a type of crystalline porous solid material, MOFs possess some distinctive features such as a periodically ordered structure, large surface area, tailored pore structure, and modifiable pore environment. These intrinsic characteristics make MOFs highly promising for gas storage and separation.[15–21] Acetylene (C_2H_2) and ethylene (C_2H_4), which are the simplest alkyne and alkene, respectively, are important feedstocks for the manufacture of a large range of industrial chemicals such as synthetic rubber, polyethylene, epoxy, and styrene. Acetylene and ethylene are generally produced from petrochemical or natural gas processing. In the production of acetylene and ethylene in the petrochemical industry through steam cracking of hydrocarbons or oxidative coupling of methane, carbon dioxide (CO_2) is the impurity in the resulting products.[22,23] Thus the removal of CO_2 impurity from the resulting mixture is important in the chemical industry for the downstream production of pure C_2H_2 and C_2H_4. The conventional technology used for CO_2 capture is the aqueous alkanolamine systems through chemical and physical absorption,[24] which suffers from high energy costs for regeneration of sorbents and serious corrosion of petrochemical equipment. However, adsorptive separations based on porous solids offer energy-efficient and environmentally friendly alternatives. MOFs have been demonstrated for CO_2 capture from gas mixtures.[25] However, most efforts are focused on the separation of binary gases such as C_2H_2/CO_2 [26–31] and C_2H_4/CO_2.[32,33] Removal of one specific gas from the ternary mixtures would simplify the separation processes and is energy-saving. However, very limited MOFs have been reported for the separation of one gas from a ternary mixture.[34–37] Thus the separation of ternary gas mixtures is largely unexplored. Due to their similar sizes (C_2H_2, 3.32 × 3.34 × 5.7 Å^3; C_2H_4, 3.3 × 4.2 × 4.8 Å^3; and CO_2, 3.18 × 3.33 × 5.36 Å^3) and close kinetic diameters (C_2H_2, 3.3 Å; C_2H_4, 4.163 Å; and CO_2, 3.3 Å) (Table S1 in the ESI†),[38] the removal of CO_2 from the ternary $C_2H_2/C_2H_4/CO_2$ mixture is a daunting challenge with a single solid physisorbent.

[a]*College of Chemistry and Chemical Engineering, Key Lab of Fluorine and Silicon for Energy Materials and Chemistry of Ministry of Education, Jiangxi Normal University, Nanchang 330022, China. E-mail: qyliuchem@jxnu.edu.cn, ylwang@jxnu.edu.cn*
[b]*Institute of Geochemistry, Chinese Academy of Sciences, Guiyang 550081, China*

†Electronic supplementary information (ESI) available. CCDC 2166003. For ESI and crystallographic data in CIF or other electronic format see DOI: https://doi.org/10.1039/d2qi01175a

‡These authors contributed equally to the work.

Results and discussion

Crystal structure

$\{[Fe_3(\mu_3\text{-}O)(DFBDC)_3(TPT)](OH)\}_n$ (JXNU-14) is crystallized in the hexagonal space group of $P6_3/mmc$ (Table S2†). The basic unit of $[Fe_3(\mu_3\text{-}O)]$ is connected by six carboxylate ligands of $DFBDC^{2-}$ and three N-containing ligands of TPT to generate a three-dimensional (3D) framework (Fig. S1, ESI†), reminiscent of its structural prototype based on the classic oxygen-centred trinuclear metal clusters.[39] The $[Fe_3(\mu_3\text{-}O)]$ unit is linked by 1,4-benzenedicarboxylate (BDC) and the TPT ligand to give $[Fe_3(\mu_3\text{-}O)(BDC)_3(TPT)]$ (MIL-88B-TPT),[40] which is the prototypical MOF of JXNU-14 with the fluorinated carboxylate ligand. The 3D structure of JXNU-14 is constructed from the trigonal bipyramidal cavities and cylindrical cavities and has one-dimensional channels with a triangular aperture (Fig. S1†). The trigonal bipyramidal cavity is composed of five $[Fe_3(\mu_3\text{-}O)]$ clusters, six $DFBDC^{2-}$ and three TPT ligands, and the cylindrical cavity consists of six $[Fe_3(\mu_3\text{-}O)]$ clusters, six $DFBDC^{2-}$ and two TPT ligands (Fig. 1). From a topological point of view, the $[Fe_3(\mu_3\text{-}O)]$ unit is linked to nine neighboring $[Fe_3(\mu_3\text{-}O)]$ through six carboxylate ligands and three TPT ligands. Thus the $[Fe_3(\mu_3\text{-}O)]$ unit can be described as a 9-connected node. Each TPT ligand bridges three $[Fe_3(\mu_3\text{-}O)]$ units and serves as a 3-connected node. As a result, the 3D framework is a binodal network with a **nia-d** topology.[41] It should be noted that the 3D framework of $[Fe_3(\mu_3\text{-}O)(DFBDC)_3(TPT)]_n$ is a cationic framework, which is charged with extra-framework species. The result of energy dispersive spectroscopy showed that no chlorine was observed in JXNU-14 (Fig. S2†). Thus the counter ions for $[Fe_3(\mu_3\text{-}O)(DFBDC)_3(TPT)]_n$ could be the hydroxide ions.

The phase purity of JXNU-14 was verified using the powder X-ray diffraction (PXRD) patterns (Fig. S3†). JXNU-14 has an accessible pore volume for guest solvent molecules, which is 53.9% of the unit cell volume. The results of the thermogravimetric analysis showed that the guest solvents in the pores can be exchanged with methanol (Fig. S4†). Thus activated JXNU-14 was obtained from the methanol-exchanged samples by evacuating at 100 °C for 23 h. On the other hand, PXRD patterns showed that JXNU-14 is stable under ambient conditions after being exposed to the air for thirty days and exhibited high water resistant stability in aqueous solutions with a wide range of pH values (1 to 11) (Fig. S3†), making it a sorbent in the practice industrial processes.

Porosity characterization

The porous structure of JXNU-14 was evaluated by N_2 adsorption isotherms. The N_2 sorption amount increased sharply with gas pressure increasing in the $0 < P/P_o < 0.01$ pressure range (Fig. 2a). Then JXNU-14 takes up N_2 slowly with a sorption amount of 355 $cm^3\ g^{-1}$ at $P/P_o = 1$. At $P/P_o = 0.01$, the N_2 uptake capacity for JXNU-14 is 310 $cm^3\ g^{-1}$, which is 87.3% of the saturation sorption amount. The adsorption and desorption curves of N_2 are completely reversible. JXNU-14 has a Brunauer–Emmett–Teller (Langmuir) surface area of 1361 $m^2\ g^{-1}$ (1527 $m^2\ g^{-1}$) and a pore volume of 0.549 $cm^3\ g^{-1}$, respectively (Fig. S5†). The pore volume is almost the same as that of 0.553 $cm^3\ g^{-1}$ derived from a single crystal structure, implying that the material is fully activated. The main cavity size distribution calculated from the sorption data using the non-localized density functional theory method is almost centred at 6.79 and 7.33 Å (Fig. 2a inset).

C_2H_2, C_2H_4 and CO_2 sorption

To assess the gas separation potential of JXNU-14, single-component gas adsorption data of C_2H_2, C_2H_4 and CO_2 were collected at 298 and 273 K (Fig. 2b and S6†). It was found that

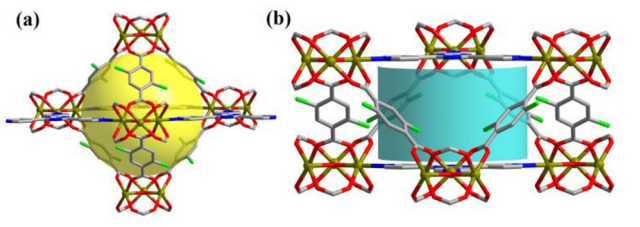

Fig. 1 (a) Trigonal bipyramidal cavity and (b) cylindrical cavity in JXNU-14 (hydrogen atoms are not shown but fluorine atoms are represented as green lines).

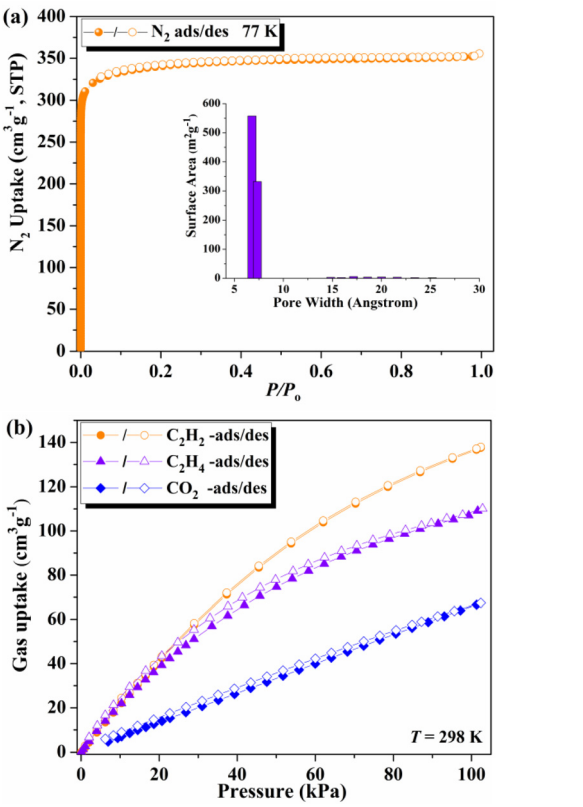

Fig. 2 (a) N_2 adsorption and desorption curves and pore cavity size distribution (inset) for JXNU-14. (b) C_2H_2, C_2H_4 and CO_2 sorption isotherms of JXNU-14.

JXNU-14 adsorbs 137.5 $cm^3\ g^{-1}$ of C_2H_2 and 110.1 $cm^3\ g^{-1}$ of C_2H_4 at 298 K and 1 bar, which are higher than those of UPC-612 (C_2H_2, 67.44 $cm^3\ g^{-1}$ and C_2H_4, 62.58 $cm^3\ g^{-1}$),[42] NTU-65 (C_2H_2, 75.4 $cm^3\ g^{-1}$ and C_2H_4, 1.2 $cm^3\ g^{-1}$),[43] UTSA-100a (C_2H_2, 95.6 $cm^3\ g^{-1}$ and C_2H_4, 37.2 $cm^3\ g^{-1}$ at 296 K),[23] and SIFSIX-17-Ni (C_2H_2, 78.5 $cm^3\ g^{-1}$ and C_2H_4, 2.2 $cm^3\ g^{-1}$)[36] under the same conditions. However, the CO_2 adsorption capacity for JXNU-14 is much low with 67.4 $cm^3\ g^{-1}$ at 298 K and 1 bar. The gas adsorption capacities for JXNU-14 follow the order of $C_2H_2 > C_2H_4 > CO_2$ at the tested temperatures. To evaluate the binding affinity of the framework for these gas molecules, the isosteric heats of adsorption (Q_{st}) were calculated from the adsorption data using the virial method (Fig. S7†). As expected, the Q_{st} values for these gas molecules follow the hierarchy of $Q_{st}(C_2H_2) > Q_{st}(C_2H_4) > Q_{st}(CO_2)$, consistent with the trend of adsorption amounts. Such a hierarchy of Q_{st} values suggests that JXNU-14 displays a stronger binding affinity to C_2H_2 and C_2H_4 than to CO_2, facilitating the preferential adsorption of C_2H_2 and C_2H_4. Such sorption behavior of JXNU-14 makes it a desirable adsorbent for the removal of CO_2 from a ternary $C_2H_2/C_2H_4/CO_2$ mixture. Moreover, JXNU-14 showed excellent recyclability for C_2H_2 and C_2H_4 adsorption, as demonstrated by the cyclic gas adsorption measurements (Fig. S8†). To further assess the separation potential of JXNU-14, adsorption selectivities of C_2H_2/CO_2 (1 : 1) and C_2H_4/CO_2 (1 : 1) mixtures were calculated using the ideal adsorbed solution theory (Fig. S9†). The calculated results showed adsorption selectivities of 2.97 for C_2H_2/CO_2 (1 : 1) and 2.60 for C_2H_4/CO_2 (1 : 1) mixtures at 298 K and 1 bar. The adsorption selectivity of the C_2H_2/CO_2 (1 : 1) mixture for JXNU-14 is comparable to those of leading MOFs such as JNU-1 (3),[44] SNNU-63 (2.7),[45] FJU-6-TATB (3.1),[46] and UTSA-68a (3.4) (Table S3†).[47] The adsorption selectivity of the C_2H_4/CO_2 (1 : 1) mixture for JXNU-14 is also comparable in comparison with those of SNNU-95 (2.4),[48] ZJNU-120(Sm) (2.4),[33] and MOF-74(Zn) (3.3),[49] but smaller than those of Ni_2(m-dobdc) (4.1)[32] and UTSA-74 (5.4) (Table S4†).[49] The coadsorption of C_2H_2 and C_2H_4 suggests that JXNU-14 is a promising candidate for the removal of CO_2 from the $C_2H_2/C_2H_4/CO_2$ mixture.

Theoretical simulations

Since the hydrogen atoms of C_2H_2 and C_2H_4 have an acidic nature, the abundant fluorine and oxygen atoms with large electronegativity on the surfaces of cavities in JXNU-14 provide a highly electrostatic potential pore environment for C_2H_2 and C_2H_4 capture, which is verified by the GCMC simulation results. As shown in Fig. 3, two energy favorable binding sites for C_2H_2 were observed. As expected, both preferential binding sites are located within the pore cavities. One is in the cylindrical cavity wherein the C_2H_2 molecule was firmly trapped through two $C–H_{(acetylene)}\cdots F$ hydrogen bonds with H···F distances of 2.53 and 2.57 Å, respectively, and two $C–H\cdots\pi_{(acetylene)}$ interactions with H···π distances of 3.74 and 3.77 Å, respectively (Fig. 3a). The other is in the trigonal bipyramidal cavity wherein the C_2H_2 molecule interacts with a framework through two $C–H_{(acetylene)}\cdots F$ (H···F = 2.81 and 2.88 Å) and two $C–H_{(acetylene)}\cdots O$ (H···O = 3.03 and 3.07 Å) hydrogen bonds (Fig. 3b). The H···F and H···O distances are comparable to the sums of van der Waals radii of H and F (2.67 Å) or H and O (2.72 Å), indicative of strong host–guest interactions. The preferential binding site for C_2H_4 is in the cylindrical cavity. C_2H_4 interacts with two F atoms of $DFBDC^{2-}$ ligands and one N atom of a TPT ligand through hydrogen bonds with H···F = 2.55 and 2.64 Å, and H···N = 3.51 and 3.52 Å, respectively (Fig. 3c). As a result, C_2H_2 and C_2H_4 molecules were firmly trapped in the pore cavities through multiple interactions, which facilitates high C_2H_2 and C_2H_4 adsorption capacities. By contrast, the pore walls with large electronegative fluorine and oxygen atoms and π systems are adverse to CO_2 adsorption because CO_2 has two large electronegative oxygen atoms. As anticipated, CO_2 weakly interacts with the framework through $C–H\cdots O_{(carbon\ dioxide)}$ (H···O = 3.31, 3.41, 3.42 and 3.48 Å) hydrogen bonds (Fig. 3d). Thus the computational results clearly demonstrated that the highly electronegative F, O and N atoms in the pore cavities synergistically attributed to the preferred adsorption of C_2H_2 and C_2H_4 over CO_2, which boost JXNU-14 with efficient removal of CO_2 from a ternary $C_2H_2/C_2H_4/CO_2$ mixture.

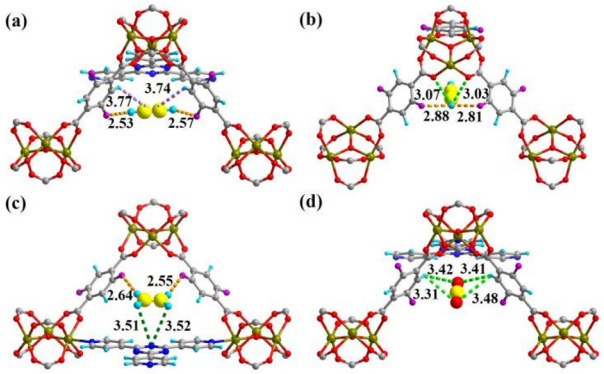

Fig. 3 The calculated preferred adsorption sites for (a) and (b) C_2H_2, (c) C_2H_4 and (d) CO_2. The unit for the labeled distance is Å. Element key: C (yellow), H (aqua) and O (red) in C_2H_2, C_2H_4 and CO_2 and C (gray), H (aqua), O (red), F (violet), and Fe (dark yellow) in JXNU-14.

Breakthrough experiments

To explore the practical gas mixture separation of JXNU-14, the separation of binary C_2H_2/CO_2 (1 : 1) and C_2H_4/CO_2 (1 : 1) mixtures was performed on JXNU-14. As depicted in Fig. 4a, the efficient separation of the C_2H_2/CO_2 mixture has been realized with JXNU-14. When a C_2H_2/CO_2 (1 : 1) mixture was fed into a column packed with activated JXNU-14, CO_2 was broken through first whereas C_2H_2 was retained in the bed. The breakthrough times for C_2H_2 are much longer than those of CO_2 at all analyzed temperatures (Fig. 4a), further demonstrating the stronger preferred affinity toward C_2H_2 over CO_2 for JXNU-14. The breakthrough intervals between C_2H_2 and CO_2 are 18.1 min g^{-1} at 298 K, 24.1 min g^{-1} at 283 K, and 27.2 min g^{-1} at 273 K, respectively, illustrating efficient C_2H_2/CO_2 separ-

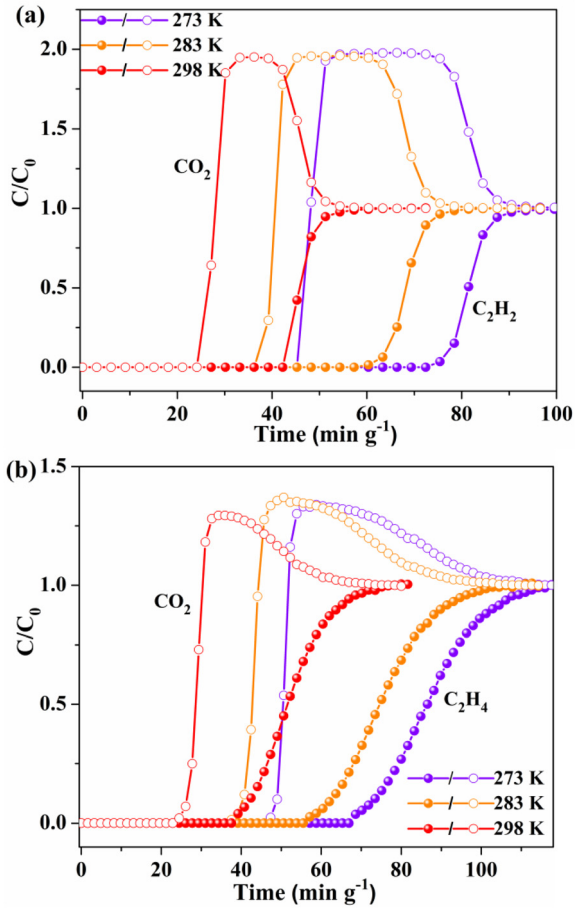

Fig. 4 Breakthrough separation of the binary (a) C_2H_2/CO_2 (1 : 1) mixture and (b) C_2H_4/CO_2 (1 : 1) mixture for JXNU-14 (total gas flow: 2 mL min^{-1}).

ation. The breakthrough time between C_2H_2 and CO_2 for JXNU-14 is similar to those of prominent MOFs of CPL-1 (14 min g^{-1}),[50] FJU-90a (22 min g^{-1}),[51] SNNU-150(Al) (20.8 min g^{-1}),[52] NKMOF-1-Ni (21 min g^{-1}),[53] and UTSA-300 (12 min g^{-1}),[54] but lower than those of leading MOFs of SNNU-45 (79 min g^{-1}),[55] JXNU-12(F) (70 min g^{-1}),[56] SIFSIX-Cu-TPA (69 min g^{-1}),[28] and JXNU-11(Fe_2Ni) (55 min g^{-1})[57] under similar conditions. As seen from the breakthrough curves (Fig. 4a), a significant CO_2 roll-up phenomenon was observed in the breakthrough experiments at all tested temperatures,[58] which suggests that the adsorbed CO_2 molecules have been largely displaced with new-coming C_2H_2 molecules. Such a roll-up phenomenon further reflects the stronger C_2H_2–framework interaction than that of the CO_2–framework. In addition, no significant change in the breakthrough times for CO_2 and C_2H_2 was observed in the three repeated measurements (Fig. S10†), demonstrating the excellent C_2H_2/CO_2 separation ability for this material. Additionally, JXNU-14 also exhibits a clean separation for the C_2H_4/CO_2 (1 : 1) mixture in the dynamic column breakthrough experiments. Likewise, the breakthrough times for C_2H_4 are longer than those of CO_2 (Fig. 4b), indicating that JXNU-14 has a preferred affinity to C_2H_4 over CO_2. The breakthrough intervals between C_2H_4 and CO_2 are 17.9 min g^{-1} at 298 K, 23.7 min g^{-1} at 283 K, and 25.9 min g^{-1} at 273 K, respectively. It is noteworthy that the CO_2 roll-up phenomenon was also observed in the breakthrough separation of the C_2H_4/CO_2 mixture. However, the roll-up behavior of CO_2 in the breakthrough separation of the C_2H_4/CO_2 mixture is weaker than that of the C_2H_2/CO_2 mixture (Fig. 4). Such a result implies that JXNU-14 has a stronger binding affinity to C_2H_2 than that of C_2H_4, in line with their isosteric heats of adsorption and the simulation results. These breakthrough results demonstrated that JXNU-14 has great potential for the separation of C_2H_2/CO_2 and C_2H_4/CO_2 mixtures.

The promising breakthrough results on the binary mixtures prompted us to further evaluate the feasibility of ternary $C_2H_2/C_2H_4/CO_2$ mixture separation. The ternary $C_2H_2/C_2H_4/CO_2$ (1 : 1 : 1) mixture was used as a feed in the breakthrough experiments. As expected, CO_2 was first eluted from the adsorbent while JXNU-14 retained C_2H_2 and C_2H_4 for a period of time (Fig. 5). The breakthrough times for C_2H_2 and C_2H_4 are 43.4 and 40.8 min g^{-1} at 298 K, respectively. The breakthrough interval between CO_2 and C_2H_4 is 16.1 min g^{-1} (298 K), demonstrating the efficient removal of CO_2 from a ternary

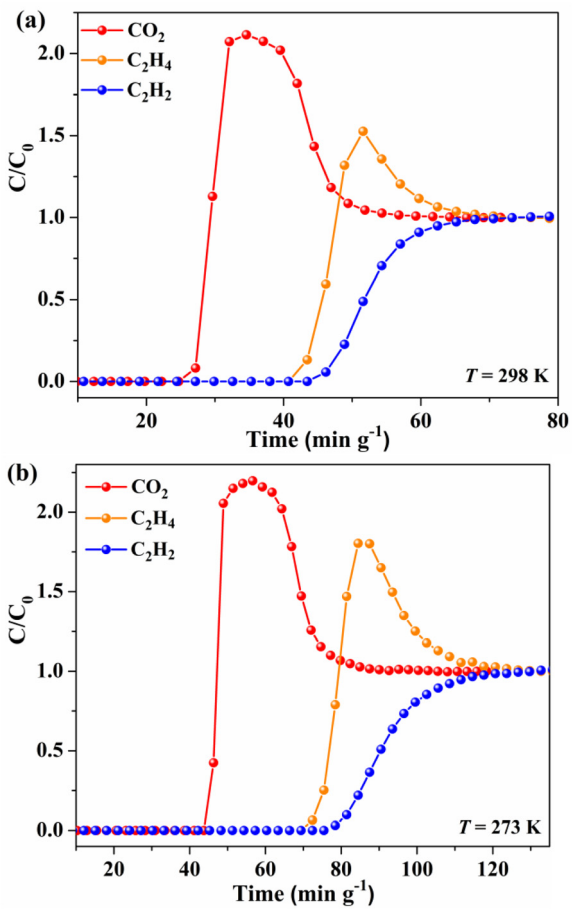

Fig. 5 Breakthrough curves for the $C_2H_2/C_2H_4/CO_2$ (1 : 1 : 1) mixture with JXNU-14 (total gas flow: 3 mL min^{-1}) (a) at 298 K and (b) 273 K.

$C_2H_2/C_2H_4/CO_2$ (1 : 1 : 1) mixture under dynamic conditions. After breaking through the bed, C_2H_2 and C_2H_4 quickly reached equilibrium. The absorbed amounts for C_2H_2, C_2H_4, and CO_2 in the column are 2.34, 1.83, and 0.59 mmol g^{-1} (Fig. S11†),[59] respectively, indicative of great efficiency for the practical removal of CO_2 from the $C_2H_2/C_2H_4/CO_2$ mixture. Furthermore, the efficient removal of CO_2 from ternary $C_2H_2/C_2H_4/CO_2$ (1 : 1 : 1) mixtures was also observed at 283 and 273 K (Fig. 5b and S12a†). Finally, no notable changes in the breakthrough times for all gases were observed in the three continuous cycling breakthrough measurements under ambient conditions (Fig. S12b†). The results of PXRD showed that JXNU-14 retained its integrity after the breakthrough experiments (Fig. S3†). Thus the JXNU-14 material showcased excellent cycling separation ability and regeneration ability, which is required for a porous solid material in industrial separation.

Conclusions

In summary, we prepared a trinuclear iron(III) based MOF of JXNU-14 constructed from the fluorinated carboxylate ligand of 2,5-difluoroterephthalate and an N-containing ligand of 2,4,6-tri(4-pyridinyl)-1,3,5-triazine. It is observed that the pore surfaces decorated with fluorine and oxygen atoms provide high-density electronegative sites, which show a stronger affinity toward C_2H_2 and C_2H_4 as compared to CO_2. JXNU-14 is capable of efficiently removing CO_2 from a ternary equimolar mixture of $C_2H_2/C_2H_4/CO_2$ as demonstrated by gas sorption experiments and breakthrough experiments. Thus the challenging separation of a ternary $C_2H_2/C_2H_4/CO_2$ mixture has been achieved using a single MOF material. This work provides an elegant example of MOF possessing densely electronegative fluorine and oxygen sites arranged on the pore surfaces for the challenging separation of a ternary $C_2H_2/C_2H_4/CO_2$ mixture.

Experimental

Materials and instruments

All chemical reagents and solvents were commercially available and used without further purification. The crystal diffraction data of JXNU-14 were collected on a Rigaku Oxford SuperNova diffractometer (Mo-Kα radiation, λ = 0.71073 Å). The crystallographic data are presented in Table S2 (ESI).† The CIF for JXNU-14 has been deposited in the Cambridge Crystallographic Data Centre (CCDC 2166003).†

Pure-component gas adsorptions were carried out with a Micromeritics ASAP 2020 HD88 sorption analyzer with high-purity gases (N_2 (99.99%), CO_2 (99.99%), C_2H_2 (99.95%) and C_2H_4 (99.999%)). The dynamic column breakthrough experiments were performed with a mixed-gas breakthrough setup with a gas chromatograph (TCD—thermal conductivity detector) continuously monitoring the effluent gas from the adsorption bed. Activated JXNU-14 (1.1601 g) was packed into a column (length: 200 mm and inner diameter: 5.0 mm) with the remaining voids filled with silica wool.

Syntheses

Synthesis of $\{[Fe_3(\mu_3\text{-}O)(DFBDC)_3(TPT)](OH)\}_n$ (JXNU-14). A mixture of 2,5-difluoroterephthalic acid (4.0 mg, 0.02 mmol), $FeCl_3{\cdot}6H_2O$ (5.4 mg, 0.02 mmol), 2,4,6-tri(4-pyridyl)-1,3,5-triazine (3.0 mg, 0.01 mmol), and 2.0 mL of *N*,*N*-dimethylformamide (DMF) was transferred into a 20 mL vial and then ultrasonicated for 15 min. The resulting solution was warmed to 100 °C for 3 days to obtain dark brown hexagonal crystals (yield 47%). Elemental analysis for $\{[Fe_3(\mu_3\text{-}O)(DFBDC)_3(TPT)](OH){\cdot}3DMF{\cdot}H_2O\}_n$ ($C_{51}H_{42}F_6O_{18}N_9Fe_3$: 1350.45): C, 45.35; H, 3.13; N, 9.33. Found: C, 45.42; H, 3.06; N, 9.21. IR data (KBr, cm^{-1}): 3420 (s), 2360 (s), 2340 (s), 1698 (m), 1683 (m), 1616 (m), 1520 (s), 1419 (s), 1373 (m), 1316 (w), 1186 (m), 1060 (m), 1022 (w), 911 (w), 863 (w), 803 (m), 774 (m), 669 (w), 653 (w).

Computational simulations

The adsorption sites of gases at 298 K were obtained from grand canonical Monte Carlo (GCMC) simulations through the fixed loading task in the sorption module. The host framework and the guest molecule were both regarded as rigid. The simulation box consisted of one unit cell and the Metropolis method based on the universal forcefield (UFF) was used. The cutoff radius was chosen as 15.5 Å for the Lennard-Jones potential, and the equilibration steps and production steps were both set as 5×10^6.

Conflicts of interest

There are no conflicts to declare.

Acknowledgements

The authors thank the National Natural Science Foundation of China (21861020 and 22061022) for the financial support. Q-Y. Liu thanks the fund for Academic and Technical Leaders of Major Disciplines of Jiangxi Province (20204BCJL22043). Y.-H. Xiao thanks the Innovation Fund (YJS2021024).

Notes and references

1 H. Li, M. Eddaoudi, T. L. Groy and O. M. Yaghi, Establishing microporosity in open metal–organic frameworks: gas sorption isotherms for Zn(BDC) (BDC=1,4-benzenedicarboxylate), *J. Am. Chem. Soc.*, 1998, **120**, 8571–8572.

2 M. Kondo, T. Yoshitomi, K. Seki, H. Matsuzaka and S. Kitagawa, Three-dimensional framework with channeling cavities for small molecules: $\{[M_2(4,4'\text{-}bpy)_3(NO_3)_4]{\cdot}xH_2O\}_n$ (M=Co, Ni, Zn), *Angew. Chem., Int. Ed. Engl.*, 1997, **36**, 1725–1727.

3 S. Ma and H.-C. Zhou, A metal–organic framework with entatic metal centers exhibiting high gas adsorption affinity, *J. Am. Chem. Soc.*, 2006, **128**, 11734–11735.
4 W. P. Lustig, S. Mukherjee, N. D. Rudd, A. V. Desai, J. Li and S. K. Ghosh, Metal–organic frameworks: functional luminescent and photonic materials for sensing applications, *Chem. Soc. Rev.*, 2017, **46**, 3242–3285.
5 L. Jiao, Y. Wang, H.-L. Jiang and Q. Xu, Metal–organic frameworks as platforms for catalytic applications, *Adv. Mater.*, 2018, **30**, 1703663.
6 W.-G. Cui, G.-Y. Zhang, T.-L. Hu and X.-H. Bu, Metal–organic framework-based heterogeneous catalysts for the conversion of C1 chemistry: CO, CO_2 and CH_4, *Coord. Chem. Rev.*, 2019, **387**, 79–120.
7 P. Horcajada, R. Gref, T. Baati, P. K. Allan, G. Maurin, P. Couvreur, G. Ferey, R. E. Morris and C. Serre, Metal–organic frameworks in biomedicine, *Chem. Rev.*, 2012, **112**, 1232–1268.
8 S. Horike, D. Umeyama and S. Kitagawa, Ion conductivity and transport by porous coordination polymers and metal–organic frameworks, *Acc. Chem. Res.*, 2013, **46**, 2376–2384.
9 L.-J. Zhou, W.-H. Deng, Y.-L. Wang, G. Xu, S.-G. Yin and Q.-Y. Liu, Lanthanide-potassium-biphenyl-3,3′-disulfonyl-4,4′-dicarboxylate frameworks: gas sorption, proton conductivity, and luminescent sensing of metal ions, *Inorg. Chem.*, 2016, **55**, 6271–6277.
10 W.-W. Zhang, Y.-L. Wang, Q.-Y. Liu and Q.-Y. Liu, Lanthanide-benzophenone-3,3′-disulfonyl-4,4′-dicarboxylate frameworks: temperature and 1-hydroxypyren luminescence sensing, and proton conduction, *Inorg. Chem.*, 2018, **57**, 7805–7814.
11 H. Li, K. Wang, Y. Sun, C. T. Lollar, J. Li and H.-C. Zhou, Recent advances in gas storage and separation using metal–organic frameworks, *Mater. Today*, 2018, **21**, 108–121.
12 M. Xie, Z. Lu, W. Lu and D. Li, Kinetic separation of C_2H_6/C_2H_4 in a cage-interconnected metal–organic framework: an interaction-screening mechanism, *Inorg. Chem. Front.*, 2022, **9**, 2697–2705.
13 Z. Dong, Y. Sun, J. Chu, X. Zhang and H. Deng, Multivariate metal–organic frameworks for dialing-in the binding and programming the release of drug molecules, *J. Am. Chem. Soc.*, 2017, **139**, 14209–14216.
14 C. Wang, D.-D. Zhou, Y.-W. Gan, X.-W. Zhang, Z.-M. Ye and J.-P. Zhang, A partially fluorinated ligand for two superhydrophobic porous coordination polymers with classic structures and increased porosities, *Natl. Sci. Rev.*, 2021, **8**, nwaa094.
15 R.-B. Lin, S.-C. Xiang, W. Zhou and B.-L. Chen, Microporous metal–organic framework materials for gas separation, *Chem*, 2020, **6**, 337–363.
16 X. Zhao, Y.-X. Wang, D.-S. Li, X.-H. Bu and P.-Y. Feng, Metal–organic frameworks for separation, *Adv. Mater.*, 2018, **30**, 1705189.
17 L.-F. Yang, S.-H. Qian, X.-B. Wang, X.-L. Cui, B.-L. Chen and H.-B. Xing, Energy-efficient separation alternatives: metal–organic frameworks and membranes for hydrocarbon separation, *Chem. Soc. Rev.*, 2020, **49**, 5359–5406.
18 T. He, X.-J. Kong and J.-R. Li, Chemically stable metal–organic frameworks: rational construction and application expansion, *Acc. Chem. Res.*, 2021, **54**, 3083–3094.
19 Z. Jiang, L. Fan, P. Zhou, T. Xu, S. Hu, J. Chen, D.-L. Chen and Y. He, An aromatic-rich cage-based MOF with inorganic chloride ions decorating the pore surface displaying the preferential adsorption of C_2H_2 and C_2H_6 over C_2H_4, *Inorg. Chem. Front.*, 2021, **8**, 1243–1252.
20 R.-B. Lin, Z.-J. Zhang and B.-L. Chen, Achieving high performance metal-organic framework materials through pore engineering, *Acc. Chem. Res.*, 2021, **54**, 3362–3376.
21 R.-B. Lin, S.-C. Xiang, W. Zhou and B.-L. Chen, Microporous metal-organic framework materials for gas separation, *Chem*, 2020, **6**, 337–363.
22 A. Granada, S. B. Karra and S. M. Senkan, Conversion of methane into acetylene and ethylene by the chlorine-catalyzed oxidative-pyrolysis (CCOP) process. 1. Oxidative pyrolysis of chloromethane, *Ind. Eng. Chem. Res.*, 1987, **26**, 1901–1905.
23 T.-L. Hu, H. Wang, B. Li, R. Krishna, H. Wu, W. Zhou, Y. Zhao, Y. Han, X. Wang, W. Zhu, Z. Yao, S. Xiang and B.-L. Chen, Microporous metal–organic framework with dual functionalities for highly efficient removal of acetylene from ethylene/acetylene mixtures, *Nat. Commun.*, 2015, **6**, 7328.
24 G. T. Rochelle, Amine Scrubbing for CO_2 Capture, *Science*, 2009, **325**, 1652–1654.
25 J.-M. Yu, L.-H. Xie, J.-R. Li, Y.-G. Ma, J. M. Seminario and P. B. Balbuena, CO_2 capture and separations using MOFs: computational and experimental studies, *Chem. Rev.*, 2017, **117**, 9674–9754.
26 W. Fan, S. Yuan, W. Wang, L. Feng, X. Liu, X. Zhang, X. Wang, Z. Kang, F. Dai, D. Yuan, D. Sun and H.-C. Zhou, Optimizing multivariate metal–organic frameworks for efficient C_2H_2/CO_2 separation, *J. Am. Chem. Soc.*, 2020, **142**, 8728–8737.
27 Y. Ye, S. Chen, L. Chen, J. Huang, Z. Ma, Z. Li, Z. Yao, J. Zhang, Z. Zhang and S. Xiang, Additive-Induced supramolecular isomerism and enhancement of robustness in Co(II)-based MOFs for efficiently trapping acetylene from acetylene-containing mixtures, *ACS Appl. Mater. Interfaces*, 2018, **10**, 30912–30918.
28 H. Li, C.-P. Liu, C. Chen, Z.-Y. Di, D.-Q. Yuan, J.-D. Pang, W. Wei, M.-Y. Wu and M.-C. Hong, An unprecedented pillar-cage fluorinated hybrid porous framework with highly efficient acetylene storage and separation, *Angew. Chem., Int. Ed.*, 2021, **60**, 7547–7552.
29 X.-P. Fu, Y.-L. Wang and Q.-Y. Liu, Metal–organic frameworks for C_2H_2/CO_2 separation, *Dalton Trans.*, 2020, **49**, 16598–16607.
30 Y. Xie, H. Cui, H. Wu, R.-B. Lin, W. Zhou and B.-L. Chen, Electrostatically driven selective adsorption of carbon dioxide over acetylene in an ultramicroporous material, *Angew. Chem., Int. Ed.*, 2021, **60**, 9604–9609.

31 J.-K. Gao, X.-F. Qian, R.-B. Lin, R. Krishna, H. Wu, W. Zhou and B.-L. Chen, Mixed metal-organic framework with multiple binding sites for efficient C_2H_2/CO_2 separation, *Angew. Chem., Int. Ed.*, 2020, **59**, 4396–4400.

32 J. E. Bachman, D. A. Reed, M. T. Kapelewski, G. Chachra, D. Jonnavittula, G. Radaelli and J.-R. Long, Enabling alternative ethylene production through its selective adsorption in the metal–organic framework Mn_2(*m*-dobdc), *Energy Environ. Sci.*, 2018, **11**, 2423–2431.

33 X.-X. Wang, L.-L. Yue, P. Zhou, L.-H. Fan and Y.-B. He, Lanthanide–organic frameworks featuring three-dimensional inorganic connectivity for multipurpose hydrocarbon separation, *Inorg. Chem.*, 2021, **60**, 17249–17257.

34 B. Zhu, J.-W. Cao, S. Mukherjee, T. Pham, T. Zhang, T. Wang, X. Jiang, K. A. Forrest, M. J. Zaworotko and K.-J. Chen, Pore engineering for one-step ethylene purification from a three-component hydrocarbon mixture, *J. Am. Chem. Soc.*, 2021, **143**, 1485–1492.

35 Y.-L. Peng, C. He, T. Pham, T. Wang, P. Li, R. Krishna, K. A. Forrest, A. Hogan, S. Suepaul, B. Space, M. Fang, Y. Chen, M. J. Zaworotko, J. Li, L. Li, Z. Zhang, P. Cheng and B.-L. Chen, Robust microporous metal–organic frameworks for highly efficient and simultaneous removal of propyne and propadiene from propylene, *Angew. Chem., Int. Ed.*, 2019, **58**, 10209–10214.

36 S. Mukherjee, N. Kumar, A. A. Bezrukov, K. Tan, T. Pham, K. A. Forrest, K. A. Oyekan, O. T. Qazvini, D. G. Madden, B. Space and M. J. Zaworotko, Amino-functionalised hybrid ultramicroporous materials that enable single-step ethylene purification from a ternary mixture, *Angew. Chem., Int. Ed.*, 2021, **60**, 10902–10909.

37 H.-G. Hao, Y.-F. Zhao, D.-M. Chen, J.-M. Yu, K. Tan, S. Ma, Y. Chabal, Z.-M. Zhang, J.-M. Dou, Z.-H. Xiao, G. Day, H.-C. Zhou and T.-B. Lu, Simultaneous trapping of C_2H_2 and C_2H_6 from a ternary mixture of $C_2H_2/C_2H_4/C_2H_6$ in a robust metal–organic framework for the purification of C_2H_4, *Angew. Chem., Int. Ed.*, 2018, **57**, 16067–16071.

38 J.-R. Li, R. J. Kuppler and H.-C. Zhou, Selective gas adsorption and separation in metal–organic frameworks, *Chem. Soc. Rev.*, 2009, **38**, 1477–1504.

39 Q.-G. Zhai, X.-H. Bu, X. Zhao, D.-S. Li and P.-Y. Feng, Pore space partition in metal–organic frameworks, *Acc. Chem. Res.*, 2017, **50**, 407–417.

40 Y.-S. Wei, M. Zhang, P.-Q. Liao, R.-B. Lin, T.-Y. Li, G. Shao, J.-P. Zhang and X.-M. Chen, Coordination templated [2+2+2] cyclotrimerization in a porous coordination framework, *Nat. Commun.*, 2015, **6**, 8348.

41 S.-T. Zheng, X. Zhao, S. Lau, A. Fuhr, P. Feng and X. Bu, Entrapment of metal clusters in metal–organic framework channels by extended hooks anchored at open metal sites, *J. Am. Chem. Soc.*, 2013, **135**, 10270–10273.

42 Y. Wang, C. Hao, W. Fan, M. Fu, X. Wang, Z. Wang, L. Zhu, Y. Li, X. Lu, F. Dai, Z. Kang, R. Wang, W. Guo, S. Hu and D.-F. Sun, One-step ethylene purification from an acetylene/ethylene/ethane ternary mixture by cyclopentadiene cobalt-functionalized metal–organic frameworks, *Angew. Chem., Int. Ed.*, 2021, **60**, 11350–11358.

43 Q. Dong, X. Zhang, S. Liu, R.-B. Lin, Y. Guo, Y. Ma, A. Yonezu, R. Krishna, G. Liu, J. Duan, R. Matsuda, W. Jin and B.-L. Chen, Tuning gate-opening of a flexible metal–organic framework for ternary gas sieving separation, *Angew. Chem., Int. Ed.*, 2020, **59**, 22756–22762.

44 H. Zeng, M. Xie, Y.-L. Huang, Y. Zhao, X.-J. Xie, J.-P. Bai, M.-Y. Wan, R. Krishna, W. Lu and D. Li, Induced fit of C_2H_2 in a flexible MOF through cooperative action of open metal sites, *Angew. Chem., Int. Ed.*, 2019, **58**, 8515–8519.

45 Y.-T. Li, J.-W. Zhang, H.-J. Lv, M.-C. Hu, S.-N. Li, Y.-C. Jiang and Q.-G. Zhai, Tailoring the pore environment of a robust Ga-MOF by deformed $[Ga_3O(COO)_6]$ cluster for boosting C_2H_2 uptake and separation, *Inorg. Chem.*, 2020, **59**, 10368–10373.

46 L. Liu, Z. Yao, Y. Ye, Y. Yang, Q. Lin, Z. Zhang, M. O'Keeffe and S. Xiang, Integrating the pillared-layer strategy and pore-space partition method to construct multicomponent MOFs for C_2H_2/CO_2 separation, *J. Am. Chem. Soc.*, 2020, **142**, 9258–9266.

47 G.-G. Chang, B. Li, H.-L. Wang, T.-L. Hu, Z.-B. Bao and B.-L. Chen, Control of interpenetration in a microporous metal–organic framework for significantly enhanced C_2H_2/CO_2 separation at room temperature, *Chem. Commun.*, 2016, **52**, 3494–3496.

48 H.-P. Li, S.-N. Li, X.-Y. Hou, Y.-C. Jiang, M.-C. Hu and Q.-G. Zhai, Enhanced gas separation performance of an ultramicroporous pillared-layer framework induced by hanging bare Lewis basic pyridine groups, *Dalton Trans.*, 2018, **47**, 9310–9316.

49 X. Zhang, H. Cui, R.-B. Lin, R. Krishna, Z.-Y. Zhang, T. Liu, B. Liang and B.-L. Chen, Realization of ethylene production from its quaternary mixture through metal–organic framework materials, *ACS Appl. Mater. Interfaces*, 2021, **13**, 22514–22520.

50 L. Yang, L. Yan, Y. Wang, Z. Liu, J. He, Q. Fu, D. Liu, X. Gu, P. Dai, L. Li and X. Zhao, Adsorption site selective occupation strategy within a metal–organic framework for highly efficient sieving acetylene from carbon dioxide, *Angew. Chem., Int. Ed.*, 2021, **60**, 4570–4574.

51 Y. Ye, Z. Ma, R.-B. Lin, R. Krishna, W. Zhou, Q. Lin, Z. Zhang, S. Xiang and B.-L. Chen, Pore space partition within a metal–organic framework for highly efficient C_2H_2/CO_2 separation, *J. Am. Chem. Soc.*, 2019, **141**, 4130–4136.

52 H.-J. Lv, Y.-P. Li, Y.-Y. Xue, Y.-C. Jiang, S.-N. Li, M.-C. Hu and Q.-G. Zhai, Systematic regulation of C_2H_2/CO_2 separation by 3p-block open metal sites in a robust metal–organic framework platform, *Inorg. Chem.*, 2020, **59**, 4825–4834.

53 Y.-L. Peng, T. Pham, P. Li, T. Wang, Y. Chen, K.-J. Chen, K. A. Forrest, B. Space, P. Cheng, M. J. Zaworotko and Z. Zhang, Robust ultramicroporous metal–organic frameworks with benchmark affinity for acetylene, *Angew. Chem., Int. Ed.*, 2018, **57**, 10971–10975.

54 R.-B. Lin, L.-B. Li, H. Wu, H. Arman, B. Li, R.-G. Lin, W. Zhou and B.-L. Chen, Optimized separation of acetylene

from carbon dioxide and ethylene in a microporous material, *J. Am. Chem. Soc.*, 2017, **139**, 8022–8028.

55 Y.-P. Li, Y. Wang, Y.-Y. Xue, H.-P. Li, Q.-G. Zhai, S.-N. Li, Y.-C. Jiang, M.-C. Hu and X.-H. Bu, Ultramicroporous building units as a path to bi-microporous metal–organic frameworks with high acetylene storage and separation performance, *Angew. Chem., Int. Ed.*, 2019, **58**, 13590–13595.

56 X.-P. Fu, Y.-L. Wang, X.-F. Zhang, R. Krishna, C.-T. He, Q.-Y. Liu and B.-L. Chen, Collaborative pore partition and pore surface fluorination within a metal–organic framework for high-performance C_2H_2/CO_2 separation, *Chem. Eng. J.*, 2022, **432**, 134433.

57 X.-P. Fu, Y.-L. Wang, X.-F. Zhang, Z.-J. Zhang, C.-T. He and Q.-Y. Liu, Fluorous metal–organic frameworks with unique cage-in-cage structures featuring fluorophilic pore surfaces for efficient C_2H_2/CO_2 separation, *CCS Chem.*, 2022, **4**, DOI: **10.31635/ccschem.021.202101575**.

58 L. J. P. Van Den Broeke and R. Krishna, Experimental verification of the Maxwell-Stefan theory for micropore diffusion, *Chem. Eng. Sci.*, 1995, **50**, 2507–2522.

59 Q. Ding, Z. Zhang, C. Yu, P. Zhang, J. Wang, X. Cui, C.-H. He, S. Deng and H. Xing, Exploiting equilibrium-kinetic synergetic effect for separation of ethylene and ethane in a microporous metal–organic framework, *Sci. Adv.*, 2020, **6**, eaaz4322.